https://doi.org/10.1016/j.compgeo.2021.104553

Effect of relative density of 2D granular materials on the arching effect through numerical trapdoor tests

Qi-Wei Liu[1,2,3,4], Han-Lin Wang[4], Ren-Peng Chen[1,2,3,*], Zhen-Yu Yin[4], Xing-Tao Lin[5], Huai-Na Wu[1,2,3]

1. Key Laboratory of Building Safety and Energy Efficiency of the Ministry of Education, Hunan University, Changsha 410082, China;
2. National Center for International Research Collaboration in Building Safety and Environment, Hunan University, Changsha 410082, China;
3. College of Civil Engineering, Hunan University, Changsha 410082, China;
4. Department of Civil and Environmental Engineering, The Hong Kong Polytechnic University, Hung Hom, Kowloon, Hong Kong, China;
5. College of Civil and Transportation Engineering, Shenzhen University, Shenzhen 518061, China;

***Corresponding author**

Prof. Ren-Peng Chen

Email: chenrp@hnu.edu.cn

Mobile: +86 13973138571

Abstract: The relative density and the fill height of granular materials influence the arching effect significantly, from either the overall behavior of granular materials or the formation of the arching effect. In this study, a comprehensive comparison of the arching effect at four fill heights with three relative densities is conducted by numerical trapdoor tests using the two-dimensional (2D) discrete element method. The results indicate that the stick-slip behavior of the arching ratio (the ratio of the average vertical stress on the trapdoor to the overburden stress; the ratio decreases to a minimum value, followed by recovering to the ultimate value) is more obvious for the case with lower fill height at a given relative density or that with higher density at a given fill height. The partial and the full arching can be distinguished by whether the loosen zone propagates to the surface. Two different critical states are identified for the partial and the full arching, respectively. These critical states are insensitive to the relative density. A characteristic height is identified around twice the width of the trapdoor, at which the critical state of the partial arching transfers to that of the full arching with the increase of the relative density.

Keywords: Arching effect; Discrete element method; Fill height; Relative density.

1. Introduction

The arching effect is a common phenomenon existing in many geotechnical applications (Terzaghi, 1943; Wang and Chen, 2019; Chen et al., 2020a), triggered by the relative movement between the stationary and mobilized portions of soils. Due to the arching effect, part of the load transfers from the mobilized portion to the stationary portion through the shear stress at the interface of these two portions. The trapdoor test is an efficient method to investigate the arching effect in granular materials, firstly developed by Terzaghi (1943). To date, such testing apparatus has been utilized in many laboratory tests to characterize the settlement field and load transfer mechanism which are related to the arching effect (Iglesia et al., 1999; Dewoolkar et al., 2007; Chevalier et al., 2009; Costa et al., 2009; Han et al., 2017; Liang et al., 2020).

The load transfer induced by the arching effect is highly affected by the soil properties (Jenck et al., 2009; Eskişar et al., 2012). Among the soil properties, the relative density D_r is an important parameter that characterizes the corresponding overall behavior of granular materials (Oda et al., 1980). During shearing, granular materials show the softening and the hardening mechanical behavior in dense and loose states, respectively. Such different mechanical behaviors affect the arching effect, induced by the shearing of granular materials. Thereby, the influence of the relative density should be considered in the arching effect. However, relevant studies remain scarce. Through a series of centrifuge tests, Dewoolkar et al. (2007) found that the minimum stress on the trapdoor of a dense sample is slightly smaller than that of the middle dense sample. A similar observation was identified by Jenck et al. (2009) based on the discrete element method. However, the deformation pattern was not mentioned at different relative densities in these two studies. On the contrary, Costa et al. (2009) proposed that the pattern of the failure mechanism in trapdoor tests was affected by the stress level and backfill density. King et al. (2019) showed that the localized (the formation of shear band) and the diffuse failure modes (shear strain develops in a non-localized mode, corresponding to the overall instability of soil) in piled embankment occurred for dense and loose samples, respectively. Nevertheless, both studies focused on the deformation pattern during the formation of the arching effect, while the variation of stress was ignored. Therefore, a comprehensive comparison between the stress and deformation patterns at different relative densities needs to be clarified.

The fill height is another crucial factor in determining the overall behavior of the arching effect. A higher fill height can provide a higher initial geostatic load next to the trapdoor, and a bigger soil volume inside two progressive shear bands induced by the movement of the trapdoor. Then, more particles are involved in the arching effect, resulting in a more effective load transfer (Fagundes et al., 2015). Furthermore, the fill height also has a significant influence on the displacement field associated with the arching effect. With the movement of the trapdoor, a loosen zone (or active zone) is generated (Zhao et al., 2021). Particles inside the loosen zone move down with the trapdoor as a whole. The “arch force bridge” (arch-like force chains) above the loosen zone is more stable than that passing through the loosen zone (Lai et al., 2018).

Therefore, the partial arching can be defined as that the loosen zone propagates to the surface and only the unstable “arch force bridge” forms. By contrast, the full arching is that the loosen zone forms inside the fill with the formation of stable “arch force bridge” above the loosen zone. Consequently, the arching effect can be classified into two patterns including the partial arching and the full arching. However, the influence of the relative density on different patterns of the arching effect is still not clear. Although Badakhshan et al. (2020) investigated the influence of the relative density on load transfer and porosity changes with different arrangements of piles, only the full arching formed in the high embankment was considered in their simulations.

In the past decades, many theoretical models have been proposed to calculate the load transfer induced by the arching effect (Terzaghi, 1943; Even, 1983; BSI 2010; EBGEO (DGGT, 2010); van Eekelen et al., 2013). In these theoretical models, the fill height is one of the predominant parameters. However, none of these models considers the relative density (or the dilation angle) of granular materials, because these models can only calculate the load transfer induced by the arching effect at the critical state (i.e., soils have reached the ultimate state). Nevertheless, the arching effect does not necessarily reach the critical state in some practical cases. As a result, it is important to understand the intermediate state of the arching effect (i.e., the evolution of load transfer with the movement of the trapdoor). Recently, some theoretical models have been proposed to reveal the progressive development of the arching effect with the movement of the trapdoor (Iglesia et al., 1999; Han et al., 2017; Rui et al., 2018). The ground reaction curve (GRC) is commonly used to present the relationship between the arching ratio and the trapdoor displacement, firstly proposed by Iglesia (1999). The GRC reflects four evolution phases of the arching ratio with the trapdoor displacement: linear and elastic (phase I), nonlinear and yielding (phase II), loading recovery (phase III) and ultimate state (phase IV). Further simplification and modification of the GRC have been proposed by Han et al., (2017) and Rui et al., (2018). However, the previous theoretical models used piecewise functions to show the GRC, instead of considering it as a continuous curve. To clarify this issue, Lin et al., (2021) proposed a continuous empirical formula to demonstrate the GRC curve. Nevertheless, the influencing factors of the fitting parameters were not discussed in their study. Meanwhile, these theoretical models are empirical, leading to some limitations to understand the evolution of the arching effect under different conditions, especially for the cases with different relative densities of granular materials coupling with different patterns of the arching effect. Therefore, the influence of the relative density and the fill height on the parameters of the formulae should be further clarified.

Numerical modelling is a useful tool to simulate the mechanical characteristics of the practical engineering cases (Han and Gabr, 2002; Wang et al., 2020). Compared with the finite element method (FEM), a particle is considered as a basic element in the discrete element method (DEM). Due to the advantages of showing the distribution of the interparticle contact force, particle displacement, and fabric, etc., the DEM has made significant contributions to studying granular materials over the last decades

(Cundall and Strack, 1979; Wang et al., 2020). Several researchers conducted DEM simulations to explore the arching effect, proving that the DEM simulation is reliable in revealing the qualitative features of the arching effect (Chevalier et al., 2009; Jenck et al., 2009; Lai et al., 2018; Badakhshan et al., 2020; Chen et al. 2020b). Although Chen et al., (2020b) demonstrated the influence of particle shape on the arching effect using two-dimensional (2D) DEM simulations, they focused on the arching effect in the piled embankment, where the interaction of the arching effect between adjacent piles could not be ignored because of the relatively small pile size compared to the trapdoor width . However, with a larger stationary part in more general cases, such as tunnels, culverts and pipes, the arching interaction between adjacent stationary parts becomes insignicant, probably inducing different load transfer mechasim and displacement field (Rui et al., 2020). Furthermore, in Chen et al., (2020b), the formation condition of the stable arch and the development of the shear band were emphasized, highly related to the effect of particle shape. Neverthless, the particle shape and the relative density are two independent influencing factors of the arching effect, which need to be investigated separately. To the authors' knowledge, the effect of relative density on the arching effect with relatively large stationary part is still an open issue.

This paper aims to unravel the role of the relative density of granular materials on the arching effect at various fill heights using 2D DEM modelling software, Particle Flow Code in Two Dimensions (PFC2D), version 5.0. For this purpose, comprehensive comparisons between loose and dense samples at different fill heights are conducted from macro to micro perspectives, including the arching ratio, the particle motion, the local porosity, the contact force, the coordination number, and the normal force fabric.

2. DEM modelling

2.1 Development of the DEM model

Compared with the three-dimensional (3D) DEM simulation, the two-dimensional (2D) DEM simulation provides high computational efficiency and maintains the key evolutions of the granular structure during the formation of the arching effect (Jenck et al., 2009; Lai et al., 2018). Also, the simulation results of 2D DEM can be directly compared with those of purely two-dimensional trapdoor tests (using the Taylor-Schneebeli soil analogues with perfect disk cross-sections as backfill). Therefore, in this study, DEM modelling is based on the purely two-dimensional trapdoor test by Xu et al. (2019). The testing setup is shown in Fig. 1 (a). The trapdoor system consists of seven blocks (B1-B7; width of each block: 128 mm), which can be moved upward and downward independently. The middle block (B4) is used as the trapdoor to move downward in Xu et al. (2019). To maintain a pure 2D condition, the backfill used in the experiment is an analogical soil of aluminium rods with different diameters (3, 4, and 5 mm), mixed at a mass ratio of 1:1:1. This kind of backfill has a uniform disk cross-section which is consistent with the basic elements (circular particle) in the 2D DEM modelling. To ensure uniform force transfer, five layers of aluminium rods with a diameter of 5 mm are laid on the blocks as a cushion. Then, the aluminium rods with different diameters are placed by layers (thickness for each layer: 20 mm) with an equal mass ratio.

Accordingly, Fig. 1 (b) shows the scheme of DEM modelling. The length of the model and the width of the trapdoor are 896 mm and 128 mm, respectively. The model height is dependent on the fill height H. Two vertical walls with a height of 25.6 mm are set on both edges of the trapdoor to prevent particles from escaping. The procedures of sample preparation in DEM modelling are listed as follows: (1) creating a testing box according to Fig. 1 (b); (2) generating the cushion layer by application of circular particles with a diameter of 5 mm in the hexagonal arrangement and fixing the velocity of these particles; (3) using the Improved Multi-layer Compaction method (Lai et al., 2014) to generate the particles by layer with approximately 20 mm thickness until the target fill height is reached; (4) setting free the velocity of cushion particles. It should be mentioned that gravity is zero during the first three steps, whereas it is restored after the target fill height is reached. The importance of employing the Improved Multi-layer Compaction method is that it is more suitable for generating homogeneous samples with different porosities and reasonable initial stress field under gravity, especially for the loose sample (Jiang et al., 2003; Lai et al., 2014).

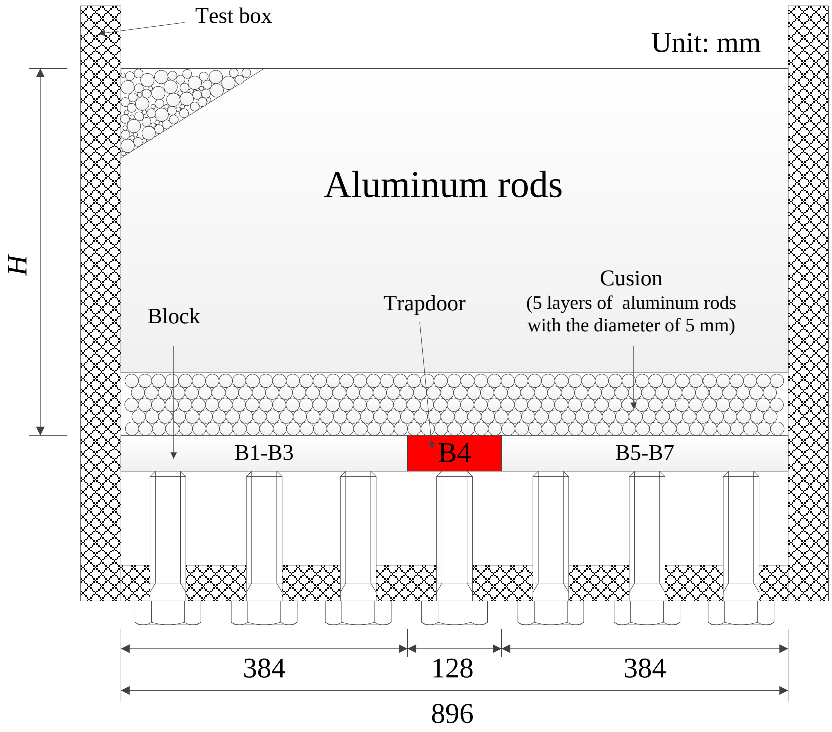

(a)

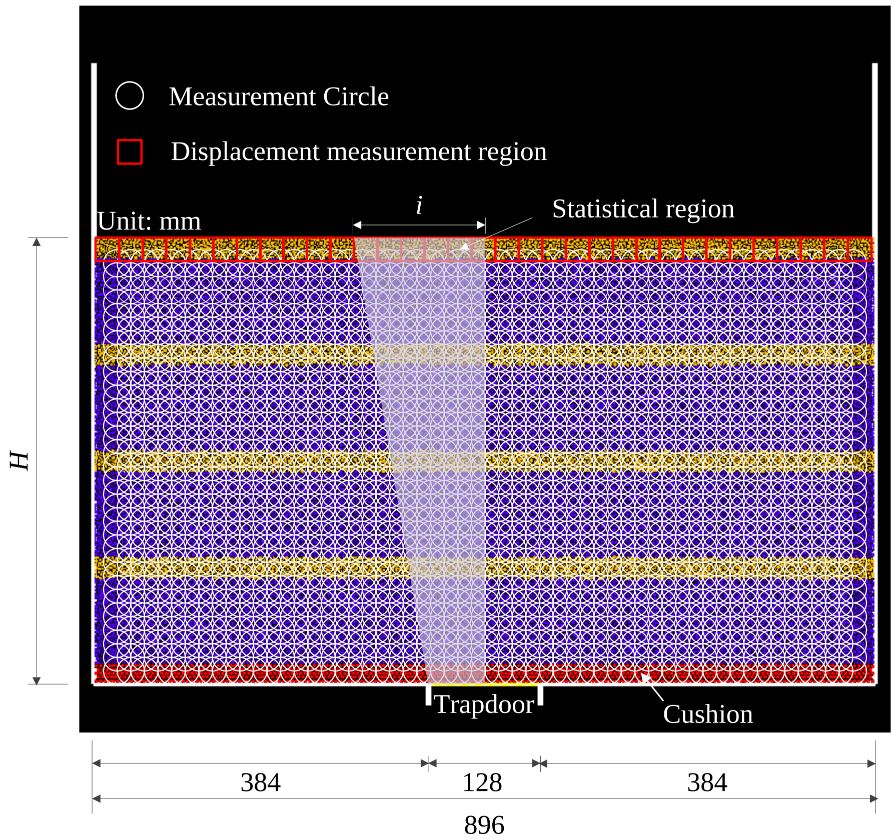

(b)

Fig. 1. (a) Testing setup used for the DEM modelling (modified from Xu et al. (2019)); (b) DEM modelling scheme

In this study, the micromechanical parameters of particles were determined from numerical biaxial tests using inverse modelling. The rolling resistance linear contact model with Coulomb sliding is applied. In the numerical biaxial tests, particles are generated in a chamber with a width of 200 mm and a height of 220 mm using the Improved Multi-layer Compaction method. The size and the proportion of particles are the same as previously demonstrated. The porosity of the samples is 0.17 as stated in the experiment (Xu et al., 2019). Different confining stresses (50 kPa, 100 kPa, and 150 kPa) are applied to the samples by a numerical servo-mechanism. As mentioned by Jenck et al. (2009), the soil strength is a dominant parameter for the arching effect in a 2D trapdoor system. Therefore, the inverse modelling from numerical biaxial experiments primarily aims to guarantee the accuracy of the strength. The comparison between numerical and experimental results of the biaxial tests is plotted in Figs. 2 (a) and 2 (b), with the micromechanical parameters listed in Table 1. The variations of the deviator stress with the axial strain in the numerical simulation shows a good agreement with those in the experiments, while the variation of the volumetric strain with the axial strain in numerical simulation shows a certain discrepancy to that of the experiment. This difference may be attributed to (1) the different sizes of the biaxial chamber [Xu et al., (2019) did not mention the size of the biaxial chamber], (2) the difference between the 2D simulation and real 3D experiment, (3) the difference between the friction of the sidewall (none friction in the simulation and with friction in the experiment). Nevertheless, the basic variation trend of the volumetric strain versus axial strain in the simulation is similar to that in the experiment. Accordingly, the inverse modelling of trapdoor tests was conducted to validate the micromechanical parameters.

Table 1. Micro-mechanical parameters used in DEM modelling

Parameter	Value
Soil	
Density of individual particle (kg/m³)	2700
Diameter (volume fraction) (mm)	3 (1/3); 4 (1/3); 5 (1/3)
Normal stiffness k_n (N/m)	8×10^5
Shear stiffness k_s (N/m)	6.8×10^5
Frictional coefficient μ	0.2
Rolling resistance coefficient μ_r	0.1
Damp	0.7
Maximum porosity n_{max}	0.204
Minimum porosity n_{min}	0.159
Wall	
Normal stiffness k_{nw} (N/m)	8.0×10^7
Shear stiffness k_{sw} (N/m)	8.0×10^7

Note: n_{max} and n_{min} are determined from the method proposed by Wood and Maeda (2007).

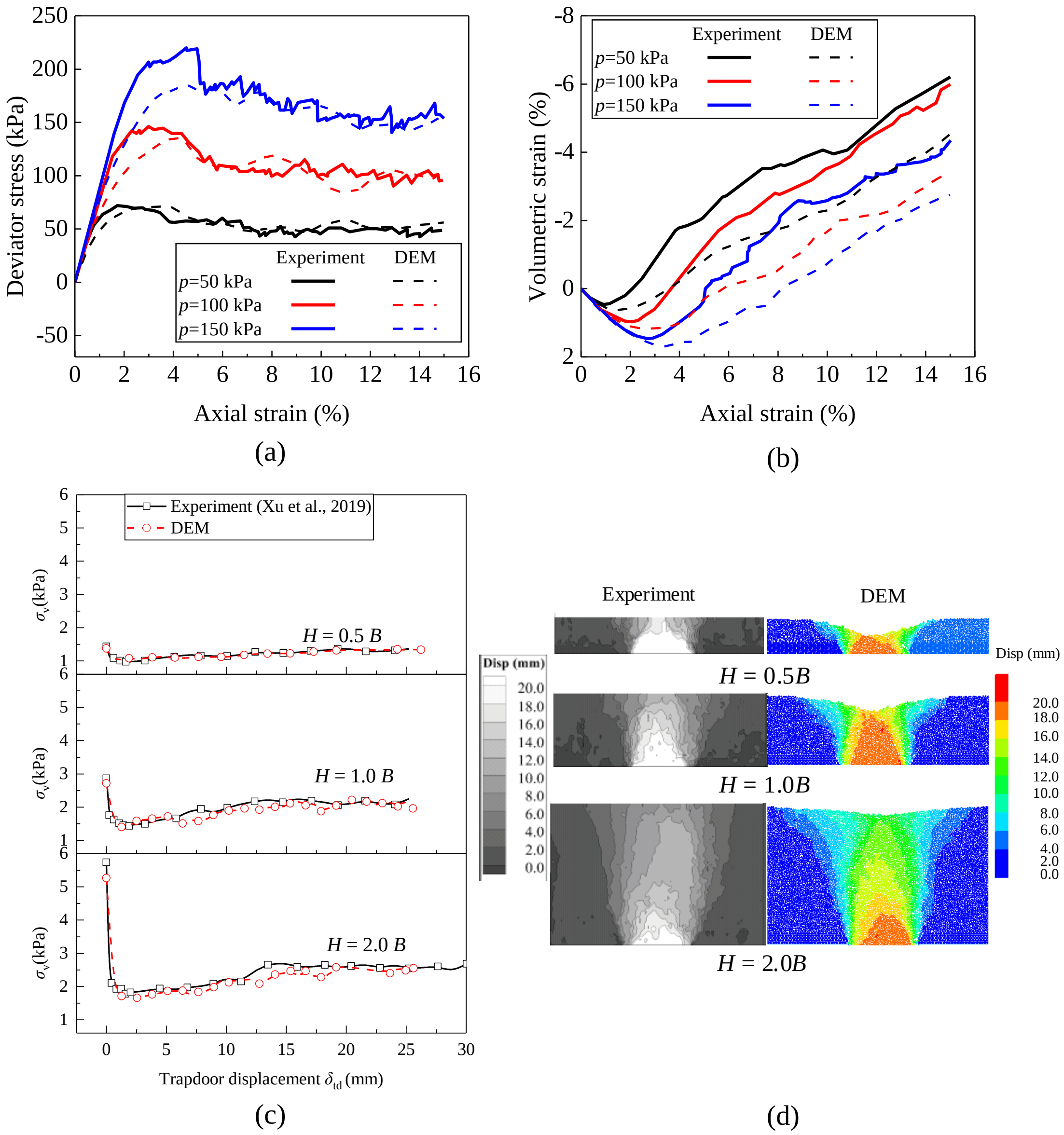

Fig. 2. Validation result of (a, b) biaxial compression tests and (c, d) trapdoor tests

Note: σ_v is average vertical pressure acting on the trapdoor; δ_{td} represents the trapdoor displacement

Figs. 2 (c) and (d) show a good consistency for numerical and experimental results of the trapdoor tests, suggesting that the selected micromechanical parameters are reliable to capture the macroscopic behavior of the aluminium rods used in the laboratory tests. Table 2 shows modelling samples in this study, including 12 cases with various fill heights and relative densities. The ratio between the fill height and the trapdoor width ranges from 0.5 to 4. Three relative densities are selected, revealing the differences of the arching effect in granular materials from the loose to the dense sample. According to the maximum and the minimum porosity listed in Table 1, the relative density D_r of the sample in DEM simulation can be calculated as (Wood and Maeda, 2007):

$$D_r = \frac{(n_{\max} - n)(1 - n_{\min})}{(n_{\max} - n_{\min})(1 - n)} \times 100\% \tag{1}$$

where n is the porosity of the sample. Using this equation, the target porosities are 0.191, 0.178, and 0.164, respectively, when the relative densities are 30%, 60%, and 90%. It can be seen from Table 2 that the difference between the initial and target porosity is less than 0.001, indicating the high accuracy of the Improved Multi-layer Compaction method. In addition, the dilation angle increases with the increase of the relative density at a given fill height. However, the dilation angle varies insignificantly with the increase of the fill height at a given relative density, which can be attributed to the minor difference of the mean effective stress (the minimum and the maximum values are 1.40 kPa and 11.56 kPa).

Table 2. Modelling samples

Specimen	B (mm)	H (mm)	Initial porosity n_{ini}	D_r (%)	Nomenclature	Dilation angle ψ (°)
S1			0.1915	30	0.5B30	7.2
S2	128	64	0.1784	60	0.5B60	8.6
S3			0.1643	90	0.5B90	10.7
S4			0.1917	30	1.0B30	7.0
S5	128	128	0.1775	60	1.0B60	8.5
S6			0.1634	90	1.0B90	10.6
S7			0.1913	30	2.0B30	7.3
S8	128	256	0.1780	60	2.0B60	8.3
S9			0.1637	90	2.0B90	10.3
S10	128	512	0.1906	30	4.0B30	7.1
S11			0.1775	60	4.0B60	8.0

S12	0.1639	90	4.0B90	10.3

Note: B is the trapdoor width; H is the fill height; n_{ini} is the initial porosity before the trapdoor movement; D_r is the relative density; ψ is the dilation angle of the soil near the trapdoor.

2.2 Testing Procedure and Measurement

In the testing stage, the trapdoor moves down at the speed of 1×10^{-7} mm per step. Both quasi-static state and high computational efficiency can be guaranteed in this downward speed of the trapdoor.

Measurement circles are set to record the local porosity in the model, as depicted in Fig. 1 (b). The diameter of each measurement circle is 32 mm, which is more than 4 times larger than the maximum diameter of the particle (5 mm) to prevent the statistical result from fluctuating (Rojek et al., 2013). Moreover, there are 14 displacement measurement regions to detect the surface settlement of the sample. The dimensions of each region are 28 mm×28 mm and the spacing of the centre region between the adjacent ones is 28 mm. The detailed demonstration and function of displacement detection can be referred to Chen et al. (2020b).

3. Numerical Results

3.1 Arching ratio and contact force

To quantitively evaluate the arching effect, the arching ratio ρ is defined as (Han and Gabr, 2002):

$$\rho=\frac{\sigma_v}{\gamma H+q_0} \tag{2}$$

where γ is the unit weight of granular materials; H is the height of the granular materials; q_0 is the surcharge on the surface; The displacement of the trapdoor is represented by normalized displacement N_{D} expressed as:

$$N_{\mathrm{D}} = \frac{\delta_{\mathrm{td}}}{B} \times 100\% \tag{3}$$

where B is the width of the trapdoor (128 mm in this study).

Fig. 3 depicts the variations of the arching ratio with normalized displacement at different fill heights. In this figure, the hollow points and the curves represent simulation data and fitting results, respectively. The fitting function is the continuous ground reaction curve (GRC) proposed by Lin et al. (2021) as:

$$\rho = 1 - b - (aN_{\mathrm{D}} - b)e^{-mN_{\mathrm{D}}^{c}} \tag{4}$$

where a, b, c, and m are fitting parameters, explained in detail as follows.

According to Equation (4), the following characteristics can be deduced:

(1) For the case of $N_{\mathrm{D}}=0$, the arching ratio ρ is 1, indicating that the fitting curve passes through (0,1) in the figure of the arching ratio versus the normalized displacement;

(2) For the case of $N_{\mathrm{D}} \to 0$, the arching ratio ρ is $(1 - aN_{\mathrm{D}})$, meaning that a represents the slope of the straight line at the beginning of the fitting curve, corresponding to the development of the arching effect at or close to the geostatic state (this slope can also be called the modulus of arching (Iglesia et al., 1999)).

(3) For the case of $N_{\mathrm{D}} \to \infty$, the arching ratio ρ is approaching the ultimate value

of $(1-b)$.

(4) According to the previous parametric analysis conducted by Lin et al. (2021), m reflects the normalized displacement corresponding to the maximum arching effect (i.e., the minimum arching ratio). The larger the value of m is, the smaller the normalized displacement is needed to reach the maximum arching effect. The strength of load recovery (i.e., the slope of the line from the minimum to the ultimate arching ratio) is more dependent on c. A larger c corresponds to the higher strength of load recovery.

It can be seen from Fig. 3 that the fitting curves show a good agreement with the simulation data. All coefficients of determination R^2 are larger than 0.70 and increase as the fill height increases. For the cases with low fill height, fewer particles participate in the shearing. Each particle around the shear band bears a large percentage of contact forces. However, because of the movement of these particles, force chains build and collapse. An abrupt fluctuation of trapdoor load occurs, resulting in low coefficients of determination. Nevertheless, the fitting curve well predicts the variation trend of the arching ratio with normalized displacement, which is sufficient for qualitative analysis. For all cases, the arching ratio decreases to the minimum value and then increases to the ultimate value with the increase of normalized displacement, with the observation namely as the stick-slip behavior (Rui et al., 2019). The stick-slip behavior is more obvious when $H < 2.0B$. At a given fill height, denser samples exhibit more obvious stick-slip behavior than looser samples.

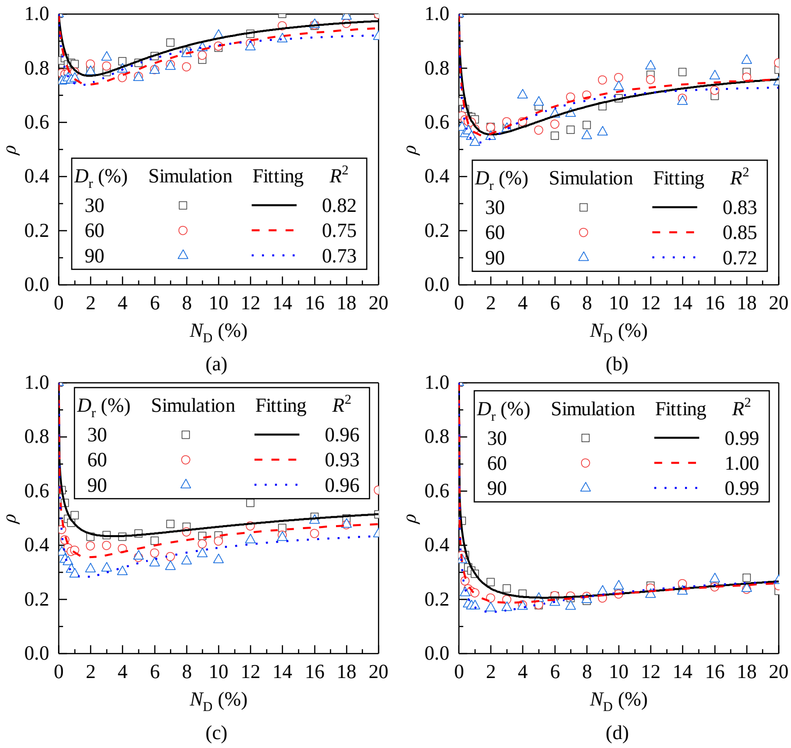

Fig. 3. Variations of the arching ratio with normalized displacement at different fill heights: (a) H= 0.5 B; (b) H= 1.0 B; (c) H= 2.0 B; (d) H = 4.0 B

To have a better understanding of the differences of the arching effect at different conditions, Fig. 4 presents the variation of fitting parameters with different fill heights at different relative densities. Fig. 4 (a) shows that a (the modulus of arching) increases with the increase of the fill height or the relative density, indicating that the arching effect develops rapidly in the large stress field or the dense sample. However, the modulus of arching of the dense sample reaches the maximum value and then remains stable with the increase of the fill height, while that of the loose sample shows continuous growth. This is because, for the loose sample, the increase of fill height will gradually compact particles close to the trapdoor at the initial state due to the large stress field induced by gravity. Therefore, the modulus of arching of the loose sample increases gradually to that of the dense sample as the fill height increases. Such compaction is more difficult for dense samples, leading to the convergence of the modulus of arching as the fill height increases. The empirical value of the modulus of arching (Iglesia et al., 1999) can be regarded as a lower boundary but is unsuitable for the loose sample with relatively low H/B.

As previously mentioned, although the ultimate soil arching ratio is $(1-b)$, this value is obtained at a relatively large trapdoor displacement ($N_{\mathrm{D}} \to \infty$), due to the lack of the limitation for the displacement required to reach the ultimate arching. However, the fitting arching ratio varies insignificantly after 20% normalized displacement. The 20% normalized displacement is a common value in many laboratory tests to obtain the ultimate value (Dewoolkar et al., 2009; Xu et al., 2019; Liang et al., 2020). Therefore, the arching ratio calculated from the fitting function at the final state of 20% normalized displacement is sufficient to be considered as the ultimate arching ratio ρ_{ult}). Fig. 4 (b) shows the decreasing trend of the ultimate arching ratio with the increase of the fill height, corresponding to the increase in load transfer capacity of the arching effect at the ultimate state. Nevertheless, except for the cases with $H = 2.0B$, other cases show that the relative density has an insignificant influence on the ultimate arching ratio. It can be deduced that, for the cases with $H < 2.0B$ and $H > 2.0B$, the partial and the full arching can be formed at the ultimate state, respectively. Two kinds of critical states corresponding to the partial and the full arching can be identified. The relative density cannot change the patterns of the arching effect (partial or full) and the critical state at these given fill heights. However, for the cases with $H=2.0B$, the partial arching develops to the full arching with the increase of the relative density, leading to the difference of the ultimate arching ratio due to the transformation of critical states. Therefore, $H=2.0B$ can be regarded as the characteristic height in which the relative density determines the pattern of the arching effect. Both calculation methods (Terzaghi, 1943; Even, 1983) show a good agreement with the ultimate arching ratio when $H \geq 2.0B$ (the full arching), but underestimate this ratio when $H < 2.0B$ (the partial arching).

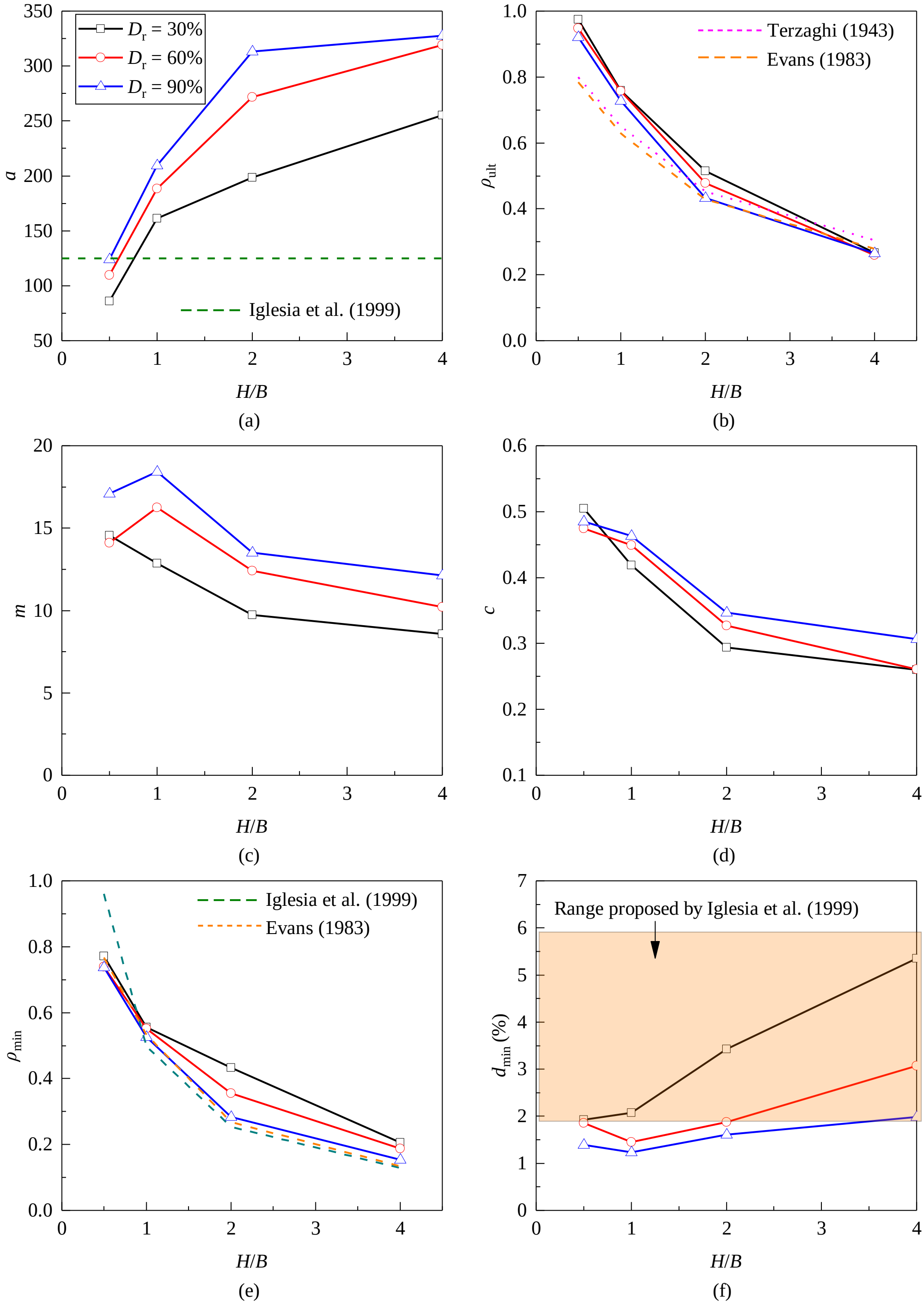

Fig. 4. Variations of fitting parameters of the arching ratio curve with different fill heights at different relative densities

Figs. 4 (c) and 4 (d) show that both m and c increase with the decrease of the fill height or the increase of the relative density. The certain fluctuation occurred on both m and c in the cases with H=0.5B is attributed to the fitting fluctuation mentioned previously. The stick-slip behavior is more obvious in lower fill height or the higher relative density. The normalized displacement corresponding to the maximum arching decreases as the fill height decreases or the relative density increases.

Figs. 4 (e) and 4 (f) represent the minimum arching ratio $\rho_{\min}$ and corresponding normalized displacement $d_{\min}$. It can be observed that the minimum arching ratio decreases with the increase of the fill height or the relative density. However, the influence of the relative density is negligible for the cases with $H < 2.0B$. The theoretical models proposed by Evens (1983) and Iglesia et al. (1999) show a good agreement with the minimum arching ratio of the dense samples in all ranges of the fill height, with better performance of the method proposed by Evens (1983). Because their theoretical models were proposed based on their trapdoor experiments with the dense sample, both theoretical models underestimate the minimum arching ratio in the loose and middle dense samples. In addition, the normalized displacement $d_{\min}$ corresponding to the minimum arching ratio shows an anti-correlation with the fitting parameter of m. The empirical range proposed by Iglesia et al. (1999) is reasonable but overestimates $d_{\min}$ for dense samples.

From a micro perspective, contact forces are the main factor controlling the stress. Figs. 5 (a) and 5 (b) show the variation of contact force at different normalized displacements, with the magnitudes of the contact force shown in the same rainbow legend. The white lines in $N_{\mathrm{D}} = d_{\min}$ are the lowest continuous force chain connecting the edges of the stationary region at the maximum arching state. It can be observed from

Fig. 5 (a) that, the contact force is almost invisible in all normalized displacements for 0.5B90. The contact force propagates from both edges of the trapdoor at the maximum arching state for 1.0B90. However, the entire “bridge” is not formed by contact forces, corresponding to the characteristics of the partial arching. By contrast, contact forces propagate from both edges of the trapdoor and form a close “bridge” for 2.0B90. According to Fig. 5 (b), the “bridge” is more obvious when $H=4.0B$. There is a region in which contact forces are relatively small below the “arch force bridge” at the maximum arching state (the region beneath the white line), resulting in a distinct release of stress in the trapdoor (i.e., a small arching ratio). The proportion of the height of this region to the fill height increases as the relative density increases or the fill height decreases. However, as the normalized displacement increases, contact forces in this region gradually recover, and force chains act directly on the trapdoor. The stick-slip behavior of the arching effect can be explained from micro perspectives as follows. The free contact force region temporarily generates beneath the “arch force bridge” at the maximum arching state because of the interlocking and the frictional resistance of particles. A further movement of the trapdoor destroys this free contact region. The greater the ratio of the height of the free contact force region to the fill height leads to the more obvious the stick-slip behavior.

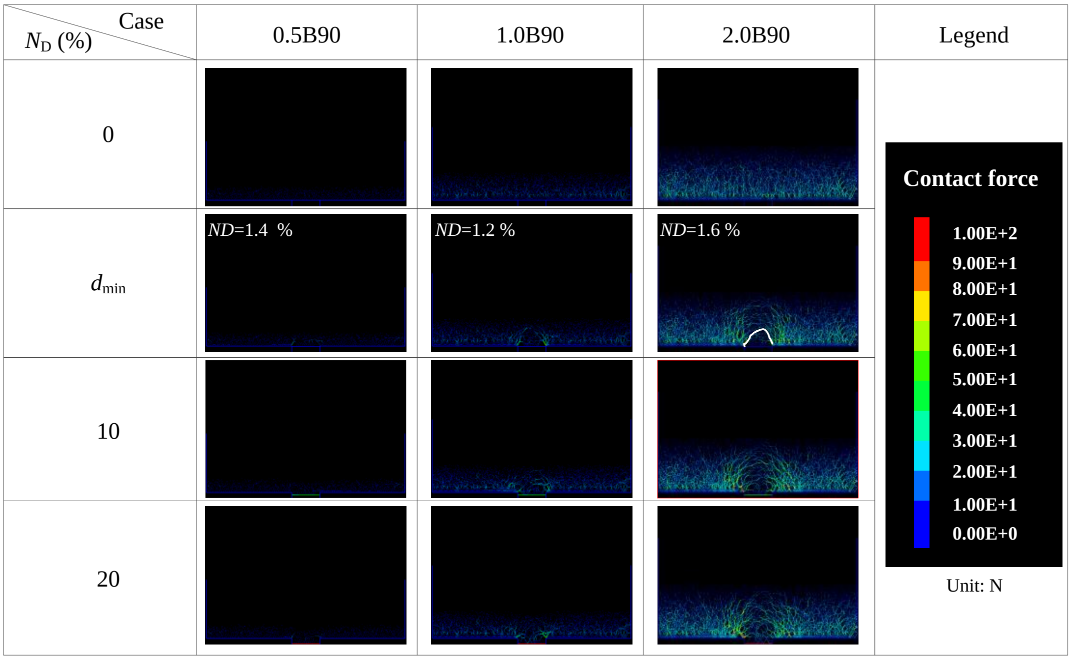

(a)

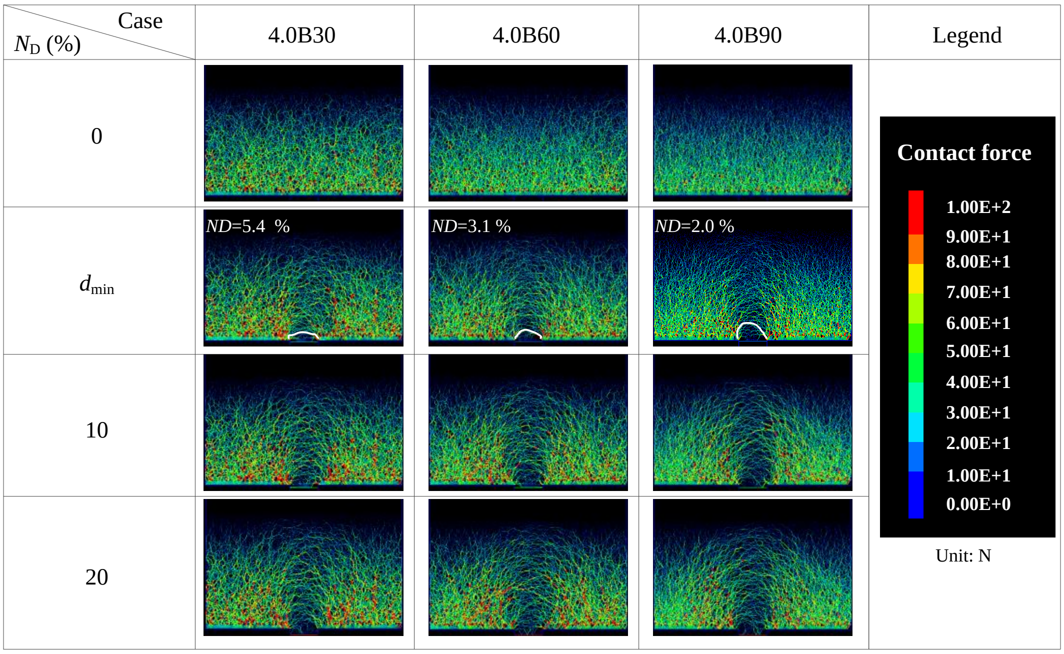

(b)

Fig. 5. Variations of contact force with (a) fill height and (b) relative density at different normalized displacement

Note: d_{min} is the normalized displacement corresponding to the minimum soil arching ratio (i.e., the maximum soil arching)

3.2 Particle motion

Fig. 6 shows the final displacement field at different fill heights and relative densities. Because the cases with H=0.5B show a similar trend as H=1.0B, the figures for H=0.5B are not shown herein. The magnitude of the displacement is represented by the colour of particles. At a given relative density, the displacement region enlarges with the increase of the fill height. On the other hand, for a constant fill height, the displacement region enlarges with the decrease of the relative density. A larger displacement region means that more particles are involved in the load transfer. Furthermore, as shown in Fig. 6 (a), the relative density only shows a slight influence on the displacement field in the cases with low fill heights, in which the loosened zone (blue part of particles) propagates from the trapdoor to the surface. Therefore, stable “arch force bridge” cannot be generated, indicating the partial arching. On the contrary, Figs. 6 (b) and 6 (c) show that the relative density has a significant effect on the displacement field in in the cases with high fill heights. For the cases with H=2.0B, the loosened zone becomes smaller with the increase of the relative density. The loosened zone of 2.0B30 is close to the surface, bringing challenges for the formation of stable “arch force bridge”. However, the loosened zone of 2.0B90 is much smaller than that of 2.0B30, indicating a suitable condition for the formation of stable “arch force bridge”. This result confirms that H=2.0B is the characteristic height in which the partial arching develops to the full arching with the increase of the relative density. Accordingly, all cases with H=4.0B show the full arching at different relative densities because the loosened zone is far from the surface. Nevertheless, the boundary of the displacement and the stationary region (i.e., the border of yellow and red) is governed by the relative density. It becomes more vertical with the increase of the relative density. This result indicates that the failure changes from diffusion to localization due to the relative density, verified by the observation from the synchrotron X-ray computed tomography test (King et al., 2019).

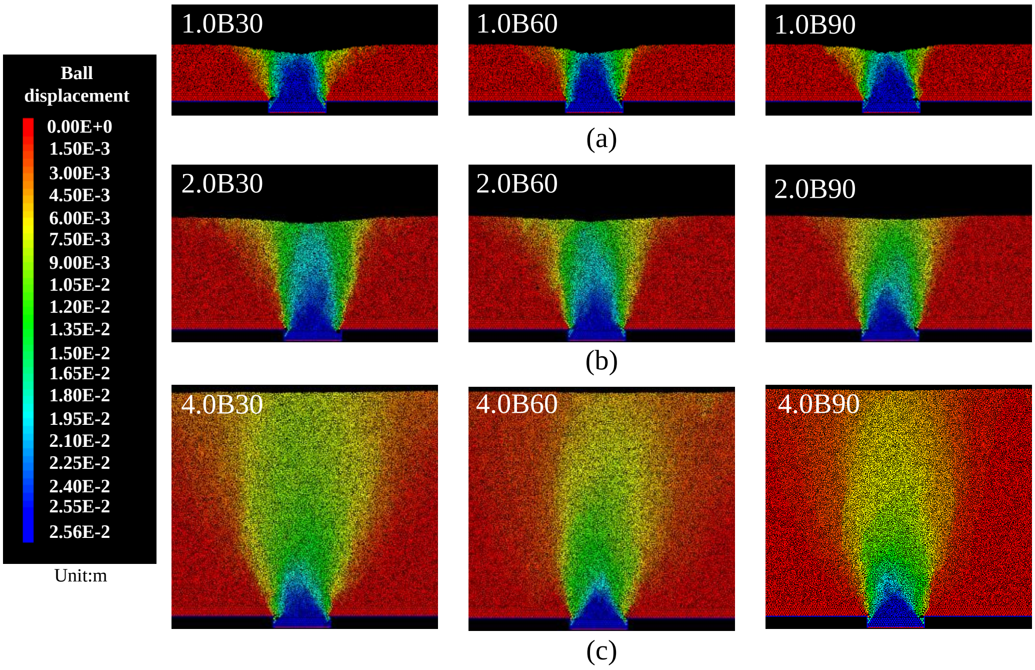

Fig. 6. The final displacement field of (a) H = 1.0 B, (b) H = 2.0 B and (c) H = 4.0 B at different relative densities

The surface settlement is another concerning issue for designers to evaluate the reliability of underground structures in geotechnical engineering. The variation of the surface settlement trough with the relative density at different fill heights is shown in Fig. 7. The simply modified Gaussian curve fitting method can be defined as (Peck, 1969):

$$S = S_0 + S_{max} \exp(-\frac{x^2}{2i^2}) \quad (5)$$

where S is the settlement of surface; S_0 means the unified displacement of surface settlement trough, which is a modified parameter compared with Peck (1969) to eliminate the influence of boundary effect; S_{max} represents the maximum vertical surface settlements; i is the horizontal distance from the centre to the inflexion point of the settlement trough.

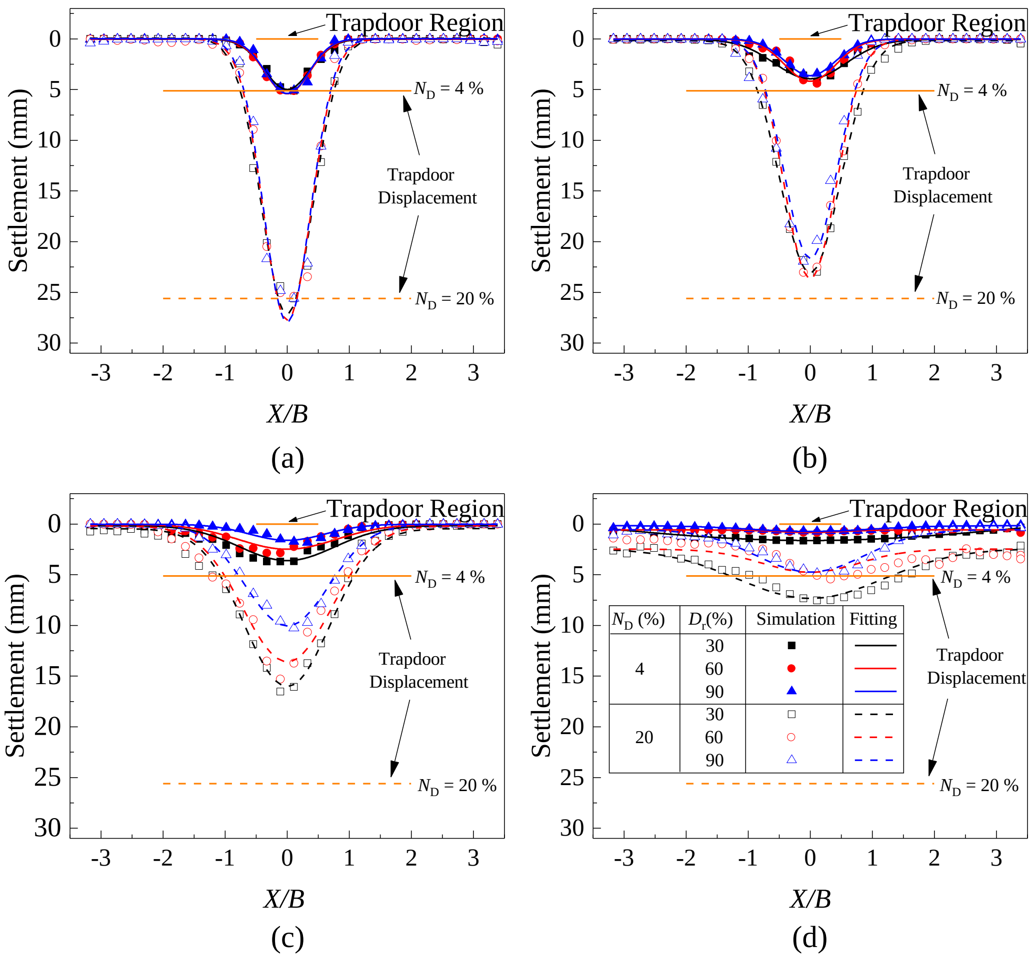

Fig. 7. Surface settlement trough of different relative densities at
(a) H =0.5 B; (b) H =1.0 B; (c) H =2.0 B and (d) H =4.0 B

Accordingly, the coefficients of determination R^2 higher than 0.85 except for 4.0B60. This exception can be attributed to the asymmetry initial defects of fabric close to the surface, but the trend of the simulation data and the fitting curve is consistent. The solid points and lines represent the simulation data and fitting results at $N_D = 4\%$

($\delta_{td} = 5.12$ mm), respectively, while hollow points and dash lines are those at $N_D = 20\%$ ($\delta_{td} = 25.6$ mm). It can be seen that, the relative density shows an insignificant influence on the development of the surface settlement when $H < 2.0\,B$, while it causes a remarkable effect when $H \geq 2.0\,B$. As illustrated by Figs. 7 (a) and 7(b), the maximum surface settlement is larger than 85% of the trapdoor displacement for the cases with low fill heights for both dense and loose samples. According to Figs. 7 (c) and 7 (d), the surface settlement decreases as the relative density increases for the cases with high fill heights. In these cases, the loosened zone cannot entirely propagate to the surface. To clarify the influence of the fill height and the relative density on the surface settlement, Fig. 8 shows the variations of fitting parameters (i and S_{max}) for the surface settlement trough at the final state ($N_D = 20\%$). i and S_{max} are normalized by the width B of trapdoor and trapdoor displacement δ_{td}, respectively. It can be observed that i/B increases as the fill height increases, but the variation trend of S_{max}/δ_{td} is opposite. This result demonstrates that the displacement region gradually widens as the fill height increases, while the maximum settlement of the surface decreases. In addition, i/B and S_{max}/δ_{td} are rarely affected by the relative density when $H < 2.0\,B$. A significant influence of the relative density occurs when $H \geq 2.0\,B$. Both parameters decrease as the increase of the relative density for a constant fill height, indicating that the displacement region narrows and the maximum settlement decreases.

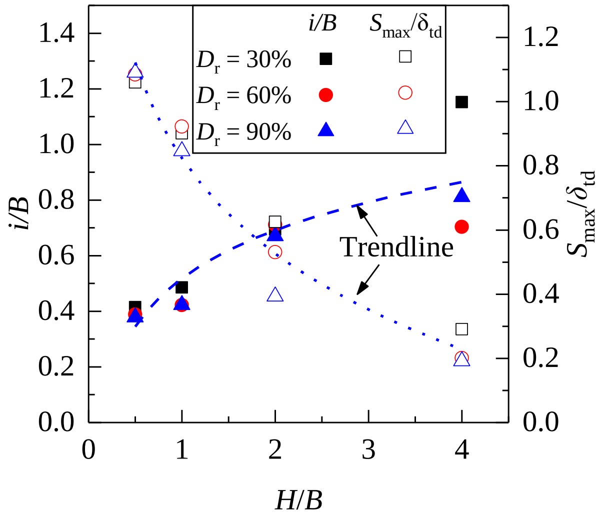

Fig. 8. Variations of fitting parameters of surface settlement trough with fill height at different relative densities

The interparticle rolling is another particle motion in controlling the strength of granular materials (Jiang et al., 2005). The high gradient of particle rotation corresponds to the boundary of the shear band (Oda and Kazama, 1998). Fig. 9 demonstrates the rotation field at the final state with different fill heights and relative densities. The high gradient of particle rotation is depicted by the blue dash line. In general, the area where the rotation of the particles is greater than 10° enlarges as the fill height increases at a given relative density. Besides, it changes from diffusion to localization as the relative density increases for a constant fill height, which is similar to the result of the displacement field. Moreover, several places present the high gradient of particle rotation, which indicates that the multiple shear band develops with the movement of trapdoor. These shear bands gradually develop upward and outward as the relative density or the fill height increases. This result has a good agreement with the illustration of the progressive development of the shear surface in the trapdoor proposed by Stone and Wood (1992).

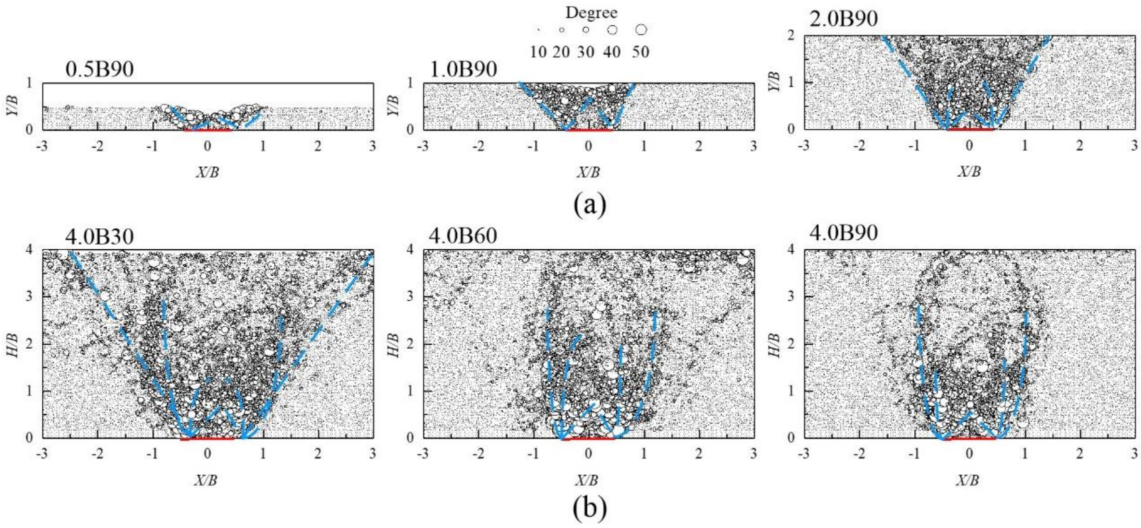

Fig. 9. Rotation field at final state with different (a) fill heights and (b) relative densities

Both the displacement and rotation of particles can be attributed to the change of contact including pure sliding, pure rolling, and a combined sliding and rolling. Fig. 10 depicts the evolution of the proportion of changing contact to the total contact at different fill heights and relative densities. It can be observed that a remarkable change of contact occurs in a relatively small normalized displacement. Moreover, the total proportion of changing contact increases with the increase of the fill height at a given relative density, indicating that more particles and contacts are included in the formation of the arching effect as the fill height increases. As shown in Fig. 10 (b), the total proportion of changing contact decreases with the increase of the relative density, demonstrating the differences between the diffuse and localized failure modes. From the micro perspective, higher relative density can effectively improve the stability of the granular system and reduce the change of contact. Therefore, the influencing range of the rotation and the displacement of particles after the movement of the trapdoor is reduced in the cases with higher density, showing localized characteristics.

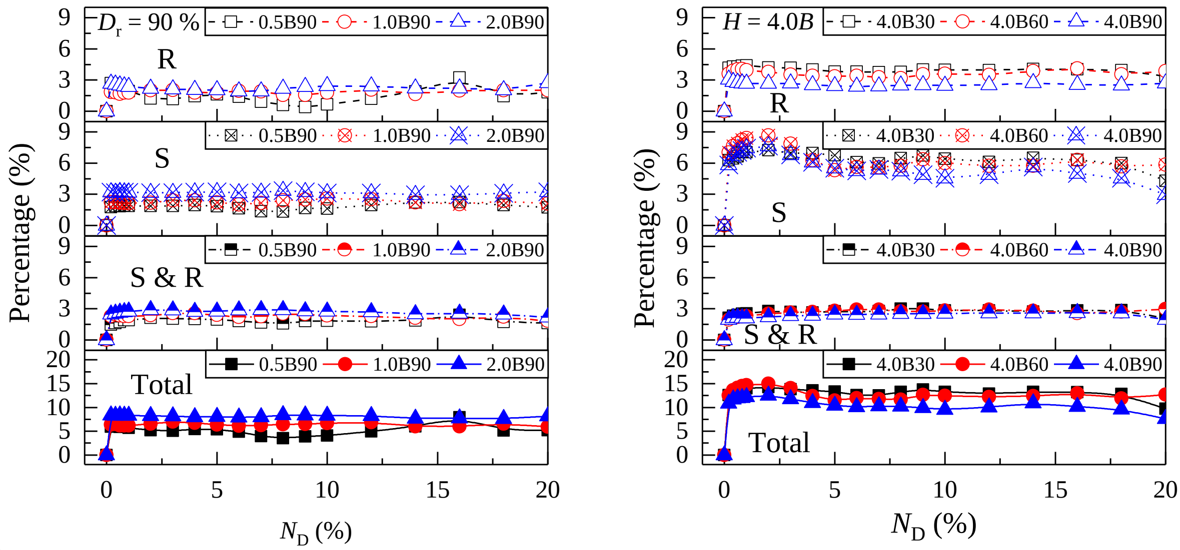

(a) (b)

Fig. 10. Evolution of the proportion of changing contact for different (a) fill heights and (b) relative densities with normalized displacement

3.3 Local porosity and Coordination number

Figs. 11 and 12 show the variation of the local porosity with different fill heights at D_r=90% and with different relative densities at H=4.0 B, respectively. The local porosity is obtained by the measurement circles, with the contour acquired by the grid data method (Chen et al., 2020b). The negative and the positive values of porosity correspond to the compression and dilation, respectively. The black lines are the boundary of compression and dilation. It can be observed from Fig. 11 that the local porosity of different fill heights is similar at the initial state due to the same relative density. At $N_D = 7\%$, a significant dilation happens near both edges of the trapdoor for all three fill heights, while the region of dilation propagates from the edges of the trapdoor to the surface for 0.5B90 and 1.0B90. Compression regions occur near the surface due to the formation of the surface settlement trough. That is, the U-shaped settlement trough causes the particles on both sides to squeeze inward, which increases the coefficient of lateral earth pressure and causes compression in this area. This phenomenon becomes less noticeable as the fill height increases. It can be interpreted as follows. As the fill height increases, the area of the U-shape surface settlement trough enlarges but the maximum settlement decreases (i increases and S_{max} decreases). Therefore, the edge slope of the settlement trough becomes gentle, leading to a smaller squeezing effect produced by the surface settlement trough and a slighter compression. Furthermore, at the final state, the surface dilation is attributed to the significant settlement around the surface. For the cases with similar initial dilation angle (Table 2), the dilation area is easier to propagate from the trapdoor to the surface for the cases with low fill height. On the other hand, as shown in Fig.12, there are some defects with high porosity (red dash circle) for 4.0B30 and 4.0B60 at the initial state. For the case of 4.0B90, the specimen becomes homogenous with fewer defects. This result means that the homogeneity of the sample increases with the increase of the relative density (or dilation angle), leading to a stronger support for the system to resist external disturbances (i.e., the movement of trapdoor). Consequently, at the final state, the porosity change area of 4.0B30 with more defects is wider than that of 4.0B60 and 4.0B90 with fewer defects. As the initial dilation angle increases, the dilation area increases, while the compression area decreases. Therefore, it can be deduced that the mechanism is different when samples with different relative densities reach the critical state.

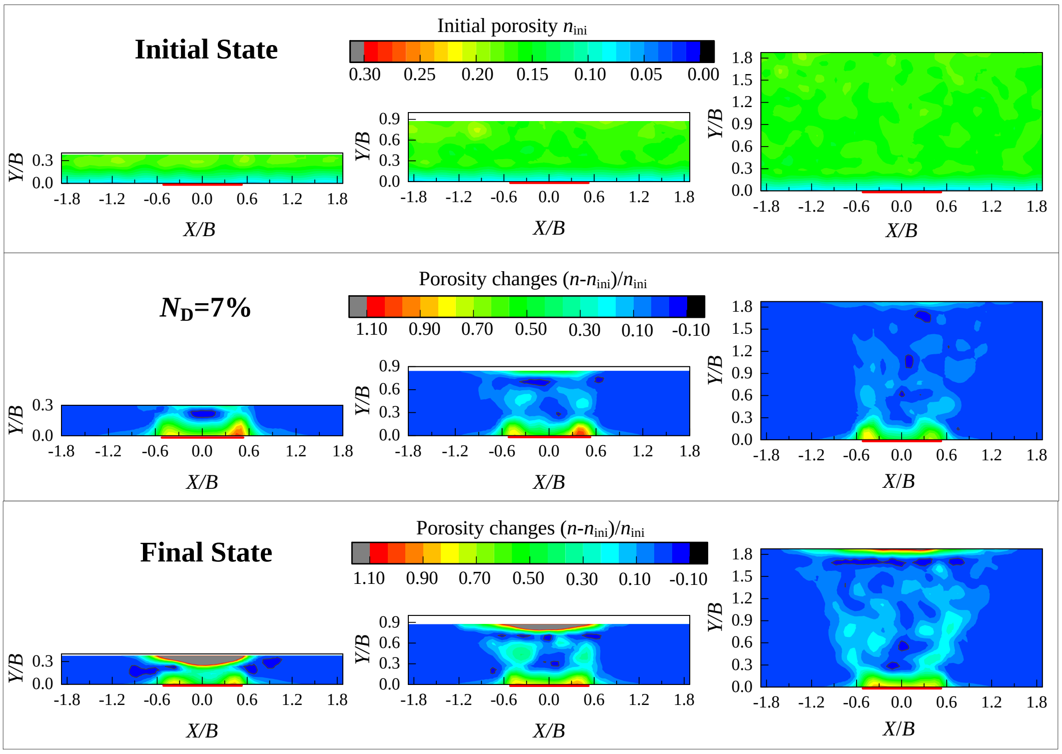

(a) (b) (c)

Fig. 11. Variations of porosity with (a) H = 0.5 B, (b) H = 1.0 B and (c) H = 2.0 B at Dr = 90%

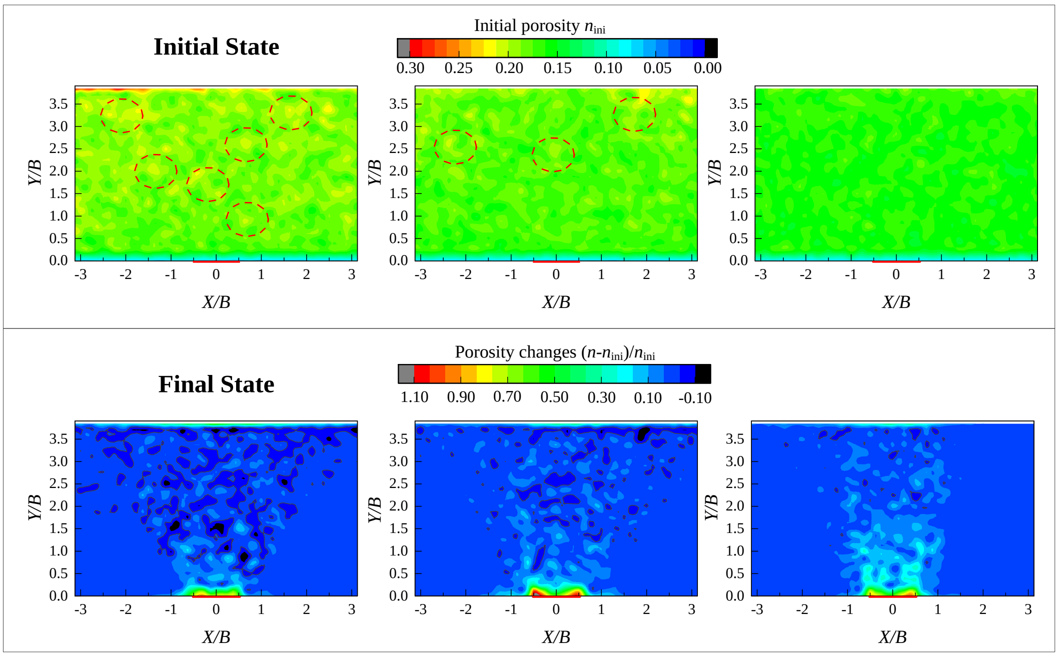

(a) (b) (c)

Fig. 12. Variations of porosity with (a) Dr = 30%, (b) Dr = 60% and (c) Dr = 90% at H = 4.0 B

To demonstrate the local porosity from the micro perspective, the average coordination number C_{N} (defined as the average contact number per particle) is used. Since the field of particle motion and porosity distribution are basically symmetrical with the centreline of the trapdoor, only half of the region from the edge of the trapdoor to the inflexion point of the settlement trough i is selected to calculate the average coordination number, as the statistical region shown in Fig. 1 (b). This statistical region can be regarded as the arching zone or displacement zone. Fig. 13 illustrates the variation of the average coordination number inside the arching zone with normalized displacement at different fill heights and relative densities. The initial coordination numbers of 0.5B90, 1.0B90, 2.0B90 and 4.0B90 are around 3.8. Nevertheless, the initial coordination number decreases with the decrease of the relative density, showing the values of 3.8, 3.63 and 3.51 for 4.0B90, 4.0B60 and 4.0B30 and, respectively. On the whole, the coordination number decreases rapidly in the beginning and then remains stable. A great fluctuation of coordination number occurs for 0.5B90 as the normalized displacement increases. There are three reasons for this phenomenon: (1) the statistical fluctuation due to the smaller numbers of balls (200) and contacts (800); (2) a more obvious compression region near the surface than other cases at $N_{\mathrm{D}} = 7\%$; (3) free movement of particles because of the small stress field (unstable state of systems). Such fluctuation disappears with the increase of fill height ($H \geq 2.0\ B$) due to the increase of the stress field and the formation of the full arching. In addition, as shown in Fig. 13 (b), the cases with different relative densities share the same average coordination number (around 3.5) at the critical state when the normalized displacement is larger than 10%, implying that the further displacement of the trapdoor (or particles) has an insignificant influence on the arching effect after reaching the critical state. Moreover, the relative density has no significant effect on the critical state.

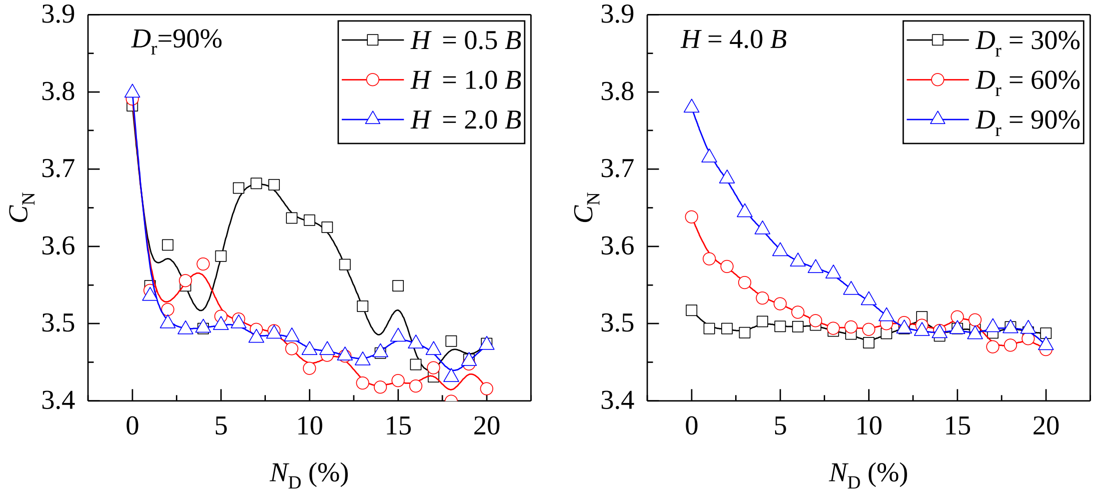

(a) (b)

Fig. 13. Variation of coordination number inside the arching zone with normalized displacement at different (a) fill heights and (b) relative densities

3.4 Normal force fabric

Polar histograms are frequently used to visualize the distribution of the contact force in various studies (Rothenburg and Bathurst, 1989), particularly for the arching effect (Lai et al., 2014) which has a close relationship to the normal force fabric (Chen et al., 2020b). Thereby, only the normal force fabric is presented in this study. The direction and the magnitude of normal contact force are collected in the same statistical region as the average coordination number and categorized at a predefined bin angle $\Delta\theta = 10°$. Meanwhile, the histogram of the normal force fabric is obtained by normalizing the normal contact force by the average normal contact force of total contacts in the statistical region. It is fitted according to a Fourier-series expansion proposed by Rothenburg and Bathurst (1989), with the detailed mathematical expression as:

$$\overline{f}_{\mathrm{n}}(\theta)=\overline{f}_0[1+a_{\mathrm{n}}\cos\ 2(\theta-\theta_{\mathrm{n}})] \tag{6}$$

where $\overline{f}_n(\theta)$ is the distribution of the average normal contact force density in the direction between $[\theta-\Delta\theta,\theta]$; $\overline{f}_0$ represents the average contact force over all contacts; a_{n} and θ_{n} are the second-order coefficient and principal direction of the normal force fabric, respectively.

Fig. 14 depicts the evolution of the normal force fabric with different fill heights at different normalized displacements. The blue dashed lines are the fitting curves according to Equation (6). The principal direction of the normal force fabric is represented by the long axis orientation of the fitting curve (red dashed-dotted lines), and the coefficient of the average normal force anisotropy is illustrated by the size of the enclosed area by the fitting curve. The initial anisotropy of normal force increases with the fill height, while its principal direction also gradually approaches the direction of gravity (vertical direction). The exception of 0.5B90 is attributed to the low-stress state, the inclined boundary of the statistical region, and fewer contacts inside the statistical region. When the arching effect develops to the maximum state ($N_{\mathrm{D}}=d_{\mathrm{min}}$), the anisotropy of normal force increases while its principal direction inclines to the right (because the statistical region is on the left side of the trapdoor). The initial vertical anisotropy transfers to a certain direction anisotropy with the formation of the arching effect, indicating the rotation of principal stress in macro perspectives. Such transformation becomes more and more obvious with the increase of the fill height. Further trapdoor movement ($N_{\mathrm{D}}=10\%$ and $N_{\mathrm{D}}=20\%$) leads to a greater fluctuation of the anisotropy of the normal force fabric, especially for the case of 0.5B90. Compared with the principal direction of the anisotropy, the magnitude of the anisotropy shows more fluctuation, suggesting that the preferred direction of contact force changes slightly but the magnitude varies significantly. However, such fluctuations are likely to be the adjustment of the contact force inside the arching zone, because they mainly occur around the preferred direction of the normal force fabric for 1.0B90 and 2.0B90. The preferred direction and the magnitude of the normal force fabric show a remarkable change compared with those at the maximum arching state in 0.5B90, demonstrating destruction of the arching effect. Such destruction leads to a large soil arching ratio (close to 1) in macro perspectives.

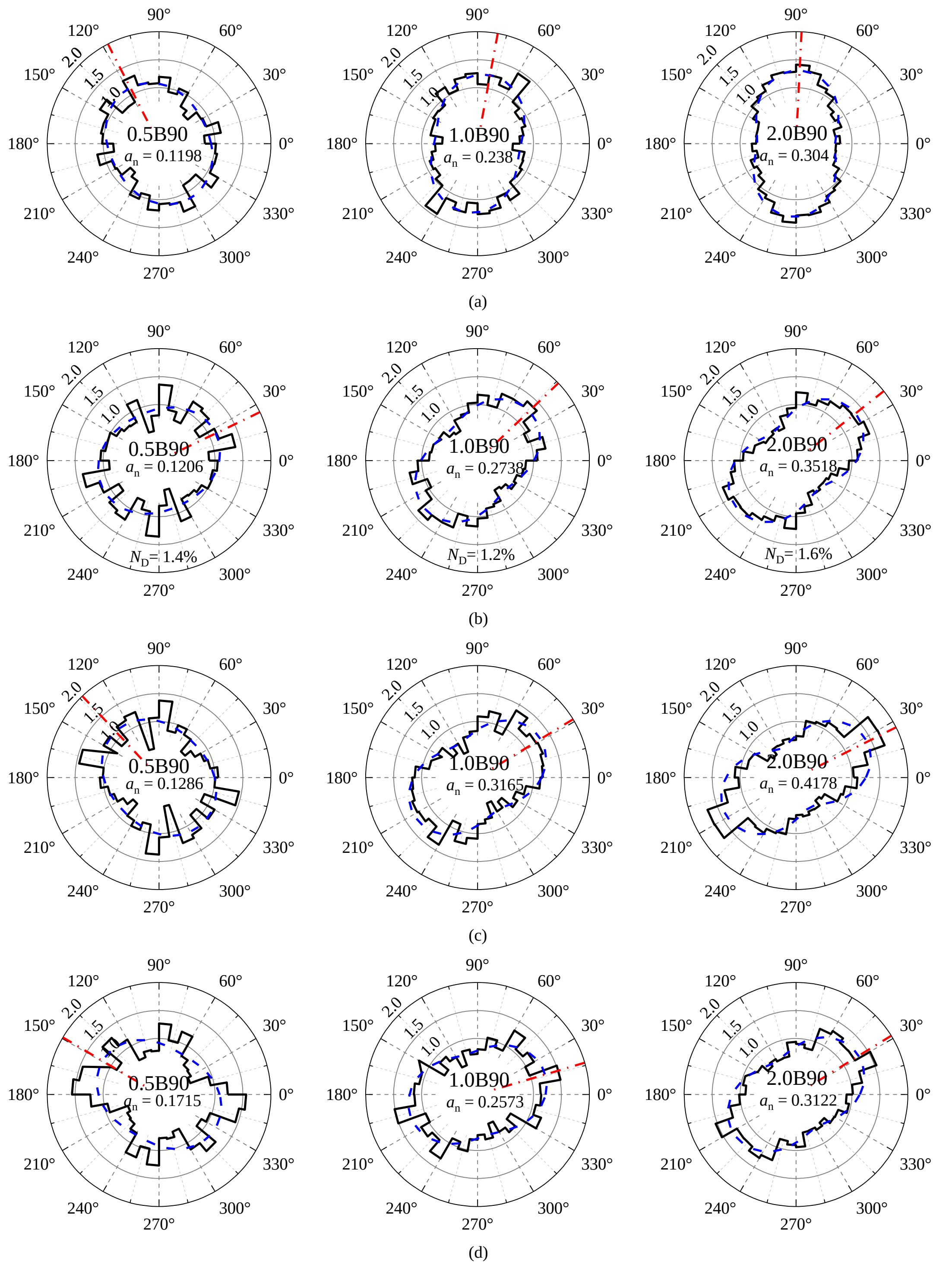

Fig. 14. The normal contact force fabric inside the arching with different fill heights at (a) $N_D = 0\%$, (b) $N_D = d_{min}$, (c) $N_D = 10\%$ and (d) $N_D = 20\%$

Fig. 15 demonstrates the evolution of the normal force fabric with different relative densities at different normalized displacements. In general, the anisotropy of the normal force fabric in the initial state aligns with the vertical axis for the cases with different relative densities (Fig. 15 (a)). However, its intensity increases with the increase of the relative density. It can be explained as follows. The loose sample has more voids than the dense sample. To maintain these voids, the contact force will extend around voids and bend along the voids, resulting in a decrease of the vertical anisotropy of the normal force fabric induced by gravity. Similar to 1.0B90 and 2.0B90, the principal direction of the normal force fabric inclines to the right at the maximum arching state (Fig. 15 (b)) for three relative densities. Accordingly, it can be concluded that most of the anisotropy of the normal force fabric rotates before the maximum arching no matter it forms a partial or a full arching. However, such rotation increases as the relative density or the fill height increases. On the other hand, the intensity of anisotropy increases from the initial state for 4.0B30 but decreases for 4.0B60 and 4.0B90 at $N_{\mathrm{D}} = d_{\min}$, which is related to the initial intensity of anisotropy of the normal force fabric induced by gravity. Nevertheless, it can be observed that the intensity of anisotropy of the normal force fabric increases faster for 4.0B60 and 4.0B90 than 4.0B30 with further movement of trapdoor after $N_{\mathrm{D}} = d_{\min}$, while the preferred direction shows a slight change. Compared with the normalized displacement ranges from 0 to $d_{\min}$, further movement of trapdoor has a less influence on the anisotropy of normal force fabric.

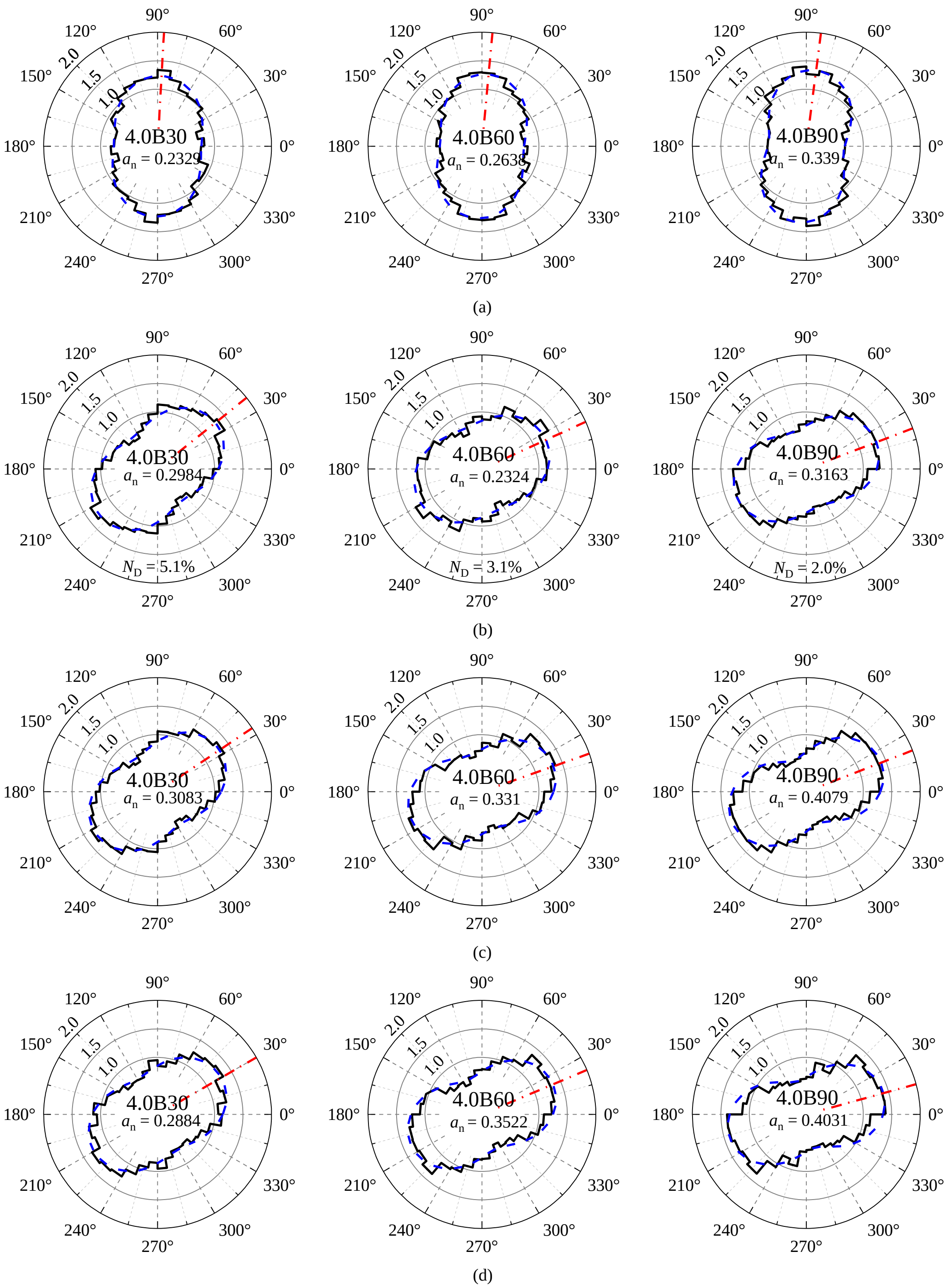

Fig. 15. The normal contact force fabric inside the arching with different relative densities at (a) $N_{\mathrm{D}}=0\%$, (b) $N_{\mathrm{D}}=d_{\min}$, (c) $N_{\mathrm{D}}=10\%$ and (d) $N_{\mathrm{D}}=20\%$

4. Discussions

From a practical point of view, the significance of this study is that providing an enhanced basis for the displacement-related theoretical model to calculate the load transfer in the intermediate state of the arching effect. Although the empirical ground reaction curve presented in this study can reflect the evolution of the arching ratio with the movement of the trapdoor, it is not a strict theoretical physical model. The stick-slip behavior of the arching ratio under different relative densities and patterns of the arching effect is clearly revealed in this study, so is the displacement field, which is beneficial to propose a strict displacement-related theoretical physical model in the future. Besides, a characteristic height is proposed to give a reference to engineers on when to consider the relative density of granular materials in practical cases associated with the arching effect. Special care should be taken when the fill height is around the characteristic height. The relative density directly determines the pattern of the arching effect and further affects the settlement and the load transfer associated with the arching effect.

Meanwhile, there are some limitations of this study. A few simplifications were made for numerical models to avoid time-consuming calculation and complicated modelling. The 3D problems, including the geometry of the trapdoor system and the spital distribution of void, were converted to 2D problems. As previously mentioned, the particle shape and the relative density are two independent influencing factors for the arching effect, which can be studied individually. This study takes a simpler particle shape to consider the influence of the relative density on the arching effect. Otherwise, the influencing parameters are not easy to be identified for the simulation results (such as the surface settlement, soil arching ratio and porosity etc.). Further studies are needed to clarify the coupling effect of the particle shape and the relative density on the arching effect.

Despite the aforementioned limitations, the evolution trend of the arching ratio with the normalized displacement in this study is similar to that in laboratory tests using sands (Iglesia et al., 1999; Chevalier et al., 2009; Liang et al., 2020). The minimum and the ultimate arching ratios are also comparable with the theoretical models (Terzaghi, 1943; Liang et al., 2020; Even, 1983). On the other hand, the variations of the displacement field with the relative density and the fill height show a good agreement with the laboratory tests from other relevant study (Moussaei et al., 2019). Therefore, the observations of this study are reasonable and significant qualitatively. Comprehensive analysis in this study shows the significant differences of the arching effect in different relative densities and patterns from macro to micro perspectives, allowing to gain insight into the mechanisms associated with the arching effect under different conditions.

5. Conclusion

Numerical trapdoor tests at four fill heights with three relative densities were conducted using the DEM to unravel the role of the relative density on the arching effect. An empirical ground reaction curve coupled with the parametric analysis was presented to reflect the arching effect at different conditions. The comprehensive comparisons from the micro to the macro perspectives at different conditions were performed in this study. The main conclusions are summarized as follows:

1. In general, with the increase of normalized displacement, the arching ratio decreases to the minimum value and then increases to the ultimate value. The empirical ground reaction curve is able to appropriately reflect the variation of the arching ratio with the normalized displacement under different conditions, which can be used to evaluate the progressive development of the arching effect.
2. For the low fill height, the diffuse failure emerges and only the partial arching forms without stable "arch force bridge". For the high fill height, the diffuse failure gradually translates to the localized failure as the relative density increases. Stable "arch force bridge" can form, corresponding to the full arching state. The partial and the full arching have corresponding critical states, respectively, while the relative density has an insignificant influence on the critical states of the arching effect.
3. A characteristic height is identified, where the relative density affects the pattern of the arching effect (H=2.0 B in this study). It is related to the dilation angle of granular materials. With the increase of the relative density, the arching effect evolves from the partial to the full state at the characteristic height, manifesting the formation of stable "arch force bridge" with the decreasing

range of the loosened zone. The characteristics of the surface settlement trough changes significantly with the relative density when the fill height is larger than the characteristic value.

4. From a micro perspective, the full arching is more stable than the partial arching according to the less fluctuation of the average coordination number on the arching zone. The average coordination number maintains constant in the arching zone after reaching the critical state, which only depends on the patterns of the arching effect and the basic characteristics of particles. The main evolution of normal force fabric occurs before the maximum arching state. This normal force fabric becomes more obvious with the increase of the relative density or the fill height.

CRediT Statement

Qi-wei Liu: Software, Formal analysis, Visualization, Writing - original draft, Writing - review and editing. **Han-lin Wang:** Validation, Writing - review and editing. **Ren-peng Chen:** Conceptualization, Supervision, Funding acquisition. **Zhen-yu Yin:** Methodology, Validation, Writing - review and editing. **Xing-tao Lin**: Methodology, Validation.

Acknowledgement

The research work described herein was funded by the National Natural Science

Foundation of China (NSFC) (Grant No. 51938005, No. 52090082). These financial supports are gratefully acknowledged.

References

Badakhshan, E., Noorzad, A., Bouazza, A., Dafalias, Y.F., Zameni, S., King, L., 2020. Load recovery mechanism of arching within piled embankments using discrete element method and small scale tests. Powder. Technol. 359, 59-75.

BSI (British Standards Institution). 2010. Code of practical for strengthened/reinforced soils and other fills. BS8006. London: BSI.

Chen, R.P., Liu, Q.W., Wang, H.L., Liu, Y., Ma, Q.L., 2020a. Performance of geosynthetic-reinforced pile-supported embankment on soft marine deposit. Proc. Inst. Civil Eng.-Geotech. Eng., 1-59. (In press)

Chen, R.P., Liu, Q.W., Wu, H.N., Wang, H.L., Meng, F.Y., 2020b. Effect of particle shape on the development of 2D soil arching. Comput. Geotech. 125, 103662.

Chevalier, B., Combe, G., Villard, P., 2009. Experimental and numerical study of the response of granular layer in the trap-door problem. Acta. Geotech. 7, 15-39.

Costa, Y.D., Zornberg, J.G., Bueno, B.S., Costa, C.L., 2009. Failure mechanisms in sand over a deep active trapdoor. J. Geotech. Geoenviron. 135, 1741-1753.

Cundall, P.A., Strack, O.D.L., 1979. A discrete numerical model for granular assemblies. Géotechnique. 29, 47-65.

Dewoolkar, M.M., Santichaianant, K., Ko, H.Y., 2007. Centrifuge modeling of granular soil response over active circular trapdoors. Soils. Found. 47, 931-945.

DGGT (German Geotechnical Society). 2010. Recommendations for design and analysis ofearth structures using geosynthetic reinforcements. Berlin: EBGEO.

Eskişar, T., Otani, J., Hironaka, J., 2012. Visualization of soil arching on reinforced embankment with rigid pile foundation using x-ray ct. Geotext. Geomembranes. 32, 44-54.

Evens C.H., 1983. An examination of arching in granular soils (M.S. thesis). MIT, Cambridge, MA.

Fagundes, D.D., de Almeida, M.D.S., Girout, R., Blanc, M., Thorel, L., 2015. Behaviour of piled embankment without reinforcement. Proc. Inst. Civil Eng.-Geotech. Eng. 168, 514-525.

Han, J., Gabr, M.A., 2002. Numerical analysis of geosynthetic-reinforced and pile-supported earth platforms over soft soil. J. Geotech. Geoenviron. 128, 44-53.

Han, J., Wang, F., Al-Naddaf, M., Xu, C., 2017. Progressive development of two-dimensional soil arching with displacement. Int. J. Geomech. 17, 04017112.

Iglesia, G. R., Einstein, H. H. & Whitman, R. V., 1999. Determination of vertical loading on underground structures based on an arching evolution concept. In Geo-

Engineering for underground facilities (pp. 495-506). ASCE.

Jenck, O., Dias, D., Kastner, R., 2009. Discrete element modelling of a granular platform supported by piles in soft soil – validation on a small scale model test and comparison to a numerical analysis in a continuum. Comput. Geotech. 36, 917-927.

Jiang, M.J., Konrad, J.M., Leroueil, S., 2003. An efficient technique for generating homogeneous specimens for DEM studies. Comput. Geotech. 30, 579-597.

Jiang, M.J., Yu, H.S., Harris, D., 2005. A novel discrete model for granular material incorporating rolling resistance. Comput. Geotech. 32, 340-357.

King, L., Bouazza, A., Dubsky, S., Rowe, R.K., Gniel, J., Bui, H.H., 2019. Kinematics of soil arching in piled embankments. Géotechnique. 69, 1-43.

Lai, H.J., Zheng, J.J., Zhang, J., Zhang, R.J., Cui, L., 2014. Dem analysis of "soil"-arching within geogrid-reinforced and unreinforced pile-supported embankments. Comput. Geotech. 61, 13-23.

Lai, H.J., Zheng, J.J., Zhang, R.J., Cui, M.J., 2018. Classification and characteristics of soil arching structures in pile-supported embankments. Comput. Geotech. 98, 153-171.

Liang, L., Xu, C., Chen, Q., Chen, Q., 2020. Experimental and theoretical investigations on evolution of soil-arching effect in 2d trapdoor problem. Int. J. Geomech. 20: 06020007.

Lin, X.T., Chen, R.P., Wu, H.N., Meng, F.Y., Liu, Q.W., Su, D. 2021. A composite function model for predicting the ground reaction curve on a trapdoor. Comput. Geotech. 125, 103662.

Moussaei, N., Khosravi, M.H., Hossaini, M.F., 2019. Physical modeling of tunnel induced displacement in sandy grounds. Tunn. Undergr. Sp. Tech. 90, 19-27.

Wood, D.M., Maeda, K., 2007. Changing grading of soil: Effect on critical states. Acta. Geotech. 3, 3-14.

Oda, M., Kazama, H., 1998. Microstructure of shear bands and its relation to the mechanisms of dilatancy and failure of dense granular soils. Géotechnique. 48, 465-481.

Oda, M., Konishi, J., Nematnasser, S., 1980. Some experimentally based fundamental results on the mechanical behaviour of granular materials. Géotechnique. 30, 479-495.

Peck R.B., 1969. Deep excavations and tunnelling in soft ground. Proc 7th Int Con SMFE. Mexico City.

Rojek, J., Karlis, G.F., Malinowski, L.J., Beer, G., 2013. Setting up virgin stress conditions in discrete element models. Comput Geotech. 48, 228-248.

Rothenburg, L., Bathurst, R.J., 1989. Analytical study of induced anisotropy in idealized granular materials. Géotechnique. 40, 665-667.

Rui, R., Han, J., van Eekelen, S.J.M., Wan, Y., 2019. Experimental investigation of soil-arching development in unreinforced and geosynthetic-reinforced pile-supported embankments. J. Geotech. Geoenviron. 145, 04018103.

Rui, R., van Tol, F., Xia, Y.Y., van Eekelen, S., Hu, G., 2018. Evolution of soil arching: 2d analytical models. Int. J. Geomech. 18, 04018056.

Rui, R., Zhai, Y.X., Han, J., van Eekelen, S.J.M., Chen, C., 2020. Deformations in trapdoor tests and piled embankments. Geosynth. Int. 27, 219-235.

Stone, K.J.L., Wood, D.M., 1992. Effects of dilatancy and particle size observed in model tests on sand. Soils. Found. 32, 43-57.

Terzaghi, K., 1943. Theoretical soil mechanics. John Wiley & Sons.

van Eekelen, S.J.M., Bezuijen, A., van Tol, A.F., 2013. An analytical model for arching in piled embankments. Geotext. Geomembranes. 39, 78-102.

Wang, H.L., Chen, R.P., 2019. Estimating static and dynamic stresses in geosynthetic-reinforced pile-supported track-bed under train moving loads. J. Geotech. Geoenviron. 145, 04019029.

Wang, P., Gao, N., Ji, K., Stewart, L., Arson, C., 2020. Dem analysis on the role of aggregates on concrete strength. Comput. Geotech. 119, 103290.

Xu, C., Zhang, X.Y., Han, J., Yang, Y., 2019. Two-dimensional soil-arching behavior under static and cyclic loading. Int. J. Geomech. 19, 04019091.

Zhao, Y., Gong, Q., Wu, Y., Zornberg, J., Tian, Z., Zhang, X., 2021. Evolution of active arching in granular materials: Insights from load, displacement, strain, and particle flow. Powder. Technol. 384, 160-175.